JOURNAL OF COMPUTATIONAL PHYSICS 49, 181–198 (1983)

Computation of Steady Laminar Flow over a Circular Cylinder with Third-Order Boundary Conditions

HAMID JAFROUDI AND H. T. YANG

University of Southern California, Los Angeles, California 90007

Received October 28, 1981; revised May 18, 1982

An analytic–numerical solution to the Navier–Stokes equations is developed for the steady laminar flow past a circular cylinder. The method of series truncation is employed to reduce the governing partial differential equation to a system of ordinary differential equations, which are then numerically integrated. The Reynolds numbers Re, based on the diameter, range from 0.4 to 40. Beyond that, the flow field should be represented by cosine as well as sine series, and is to be treated later. The accuracy of the solution is enhanced by third-order boundary conditions at infinity. Quantities of interest such as the drag and pressure coefficients, tangential and radial velocities, streamlines, and vorticity lines are computed, plotted, and compared with previous results. Applying Shanks' transformation to each of three successive truncations improves the accuracy of the surface quantities.

1. INTRODUCTION

The study of laminar flow past an obstacle was pioneered by Stokes [23] who could not find the steady solution to satisfy the linearized Navier–Stokes equations. This problem, known as Stokes' paradox, remained unsolved until Oseen [19] considered the inertial terms in the Navier–Stokes equations. Imai [8] improved the asymptotic behavior of Oseen flow at a considerable distance from a cylinder immersed in uniform flow. Imai's result completely explained Filon's well-known paradox that the moment of a cylinder immersed in viscous flow is logarithmically infinite with increasing extent of the flow region. In two separate studies, Kaplun [11] and Proudman and Pearson [20] generated a procedure to calculate the higher-order approximation for low Reynolds numbers by matching two asymptotic expansions, one near the cylinder and the other far from the cylinder. Chang [3] investigated the same method of solving the flow field at great distances from an object moving through a two-dimensional steady incompressible flow. The domain of interest was considered to be infinite, and the only boundary for the fluid was the given object.

One of the earlier numerical solutions of Navier–Stokes equations was investigated by Thom [25], for low Reynolds number flow of water and oil past a circular cylinder. Kawaguti [12] integrated numerically the full Navier–Stokes equations for circular cylinder at Reynolds number 40. He found that steady flow exists even at

0021-9991/83/020181-18$03.00/0

this high Reynolds number, and that the pressure and drag coefficients conform with experimental results. By applying Imai's asymptotic solutions at infinity and using the iterative method of solving finite difference equations, Takami and Keller [24] solved the same problem for Reynolds numbers ranging from 1 to 60. Their results were in good agreement with available numerical and experimental results. Recently, Fornberg [6], using a numerical technique based on Newton's method, obtained a solution up to Reynolds number 300. Another numerical approach to this problem is the finite element method by Tuann and Olson [27] for Reynolds numbers from 1 to 100.

A useful procedure for solving nonlinear partial differential equations is the semianalytic method of series truncation or spectral method. Underwood [28] used this method for the steady flow past a circular cylinder for the range of Reynolds numbers from 0.4 to 10. The boundary conditions at infinity are from Oseen's model investigated by Van Dyke [29]. Nieuwstadt and Keller [15] used the same scheme and employed the first term in the Oseen flow obtained by Imai [8] as the improved boundary conditions at infinity for Reynolds numbers ranging from 1 to 40.

The purpose of the present work is to apply the series truncation method with third-order boundary conditions developed by Chang to the steady viscous incompressible flow past a circular cylinder. By series truncation, the governing partial differential equation is reduced to a large system of nonlinear ordinary differential equations. There are two novel features in their solution. First, Chang's Navier–Stokes solutions at great distances from a finite body transformed to series truncation, accurate to the third-order, are used as boundary conditions at large distance. Second, the two-point boundary value problem is solved by an efficient algorithm developed by Ojika [16]. In addition, application of Shanks' transformation [22] improves the accuracy of the drag and pressure coefficients, surface vorticity, and separation angle.

The computer-plotted results of streamlines, vorticity lines, tangential and radial velocities, pressure and drag coefficients, eddy length, and separation angle are compared with available experiments and other numerical and analytical solutions.

2. Flow Equations

The cylinder is placed in an incompressible laminar flow of uniform free-stream velocity U_∞. The origin of the coordinates is fixed at the center of the cylinder. The cylinder is long enough so that the change of variables in the direction of the axis of the cylinder may be ignored. The cylindrical polar coordinate system of r and θ are employed. The ordinate r is the distance of each point in the flow from the axis of the cylinder and θ represents the polar angle measured from the front stagnation point.

The vorticity transport equation nondimensionalized with reference to free stream and the radius of cylinder is [14]

$$\nabla^4\psi + \frac{\mathrm{Re}_a}{r}\left(\frac{\partial\psi}{\partial\theta}\frac{\partial}{\partial r} - \frac{\partial\psi}{\partial r}\frac{\partial}{\partial\theta}\right)\nabla^2\psi = 0, \tag{1}$$

where the Reynolds number Re_a based on the radius a of the cylinder is defined by

$$\mathrm{Re}_a = \rho U_\infty a/\mu = U_\infty a/\nu \tag{2}$$

and the stream function $\psi(r, \theta)$ is defined such that

$$u_r(r, \theta) = -(1/r)(\partial\psi(r, \theta)/\partial\theta), \tag{3}$$

$$u_\theta(r, \theta) = \partial\psi(r, \theta)/\partial r. \tag{4}$$

The only nonvanishing component of vorticity can be written as

$$\omega(r, \theta) = \frac{1}{r}\frac{\partial}{\partial r}(ru_\theta) - \frac{1}{r}\frac{\partial u_r}{\partial\theta} = \nabla^2\psi. \tag{5}$$

The boundary conditions are no-slip conditions at the surface of the cylinder,

$$\left.\begin{aligned} \psi(r, \theta) &= 0, \\ (\partial\psi/\partial r)(r, \theta) &= 0, \end{aligned}\right\} \quad \text{at} \quad r = 1, \tag{6, 7}$$

and the uniform free stream condition far from the body surface,

$$\psi(r, \theta) \sim r_\infty \sin\theta, \qquad \text{as} \quad r \to \infty. \tag{8}$$

Fourth-order partial differential equation (1), with boundary conditions (6)–(8), describes the flow pattern under consideration. Boundary condition (8) at infinity will be replaced by asymptotic behavior of the flow to the third order, as in Section 4.

3. Method of Series Truncation

The preceding system of (1), (6)–(8) is solved by the analytic–numerical method of series truncation. The stream function is expanded into a Fourier sine series

$$\psi(r, \theta) = \sum_{n=1}^{\infty} g_n(r) \sin n\theta \tag{9}$$

with functions $g_n(r)$, $n = 1, 2,...$ to be determined. In the present study, only the Fourier sine series is chosen because of flow symmetry at low Reynolds number. Substituting (9) into (1) and then equating like Fourier coefficients, we obtain the following system:

$$\sum_{i=1}^{\infty} G_i(r, g_1, g_2,...; \mathrm{Re}_a) \sin i\theta = 0, \tag{10}$$

where $G_i(r, g_1, g_2,...; \mathrm{Re}_a)$, $i = 1, 2,...$ are sets of nonlinear ordinary differential expressions. Satisfaction of (10) for arbitrary θ requires that the coefficient G_i be set

to zero for $i = 1, 2,....$ The subscript i in (10) represents the ith order of the problem. Thus, the following sets of ordinary differential equations must be solved simultaneously:

$$G_i(r, g_1, g_2,...; \mathrm{Re}_a) = 0, \qquad i = 1, 2,.... \tag{11}$$

Inside the parentheses are included the functions $g(r)$ and their derivatives to the fourth order.

The effect of the ellipticity of (11) is seen as the first-order problem is governed by the ordinary differential equation $G_1 = 0$, the second-order problem by $G_2 = 0$, etc.; and the problem of each order contains functions dependent upon higher-order problems. On the other hand, this effect does not appear in the parabolic or hyperbolic problem.

In the method of series truncation, the firt-order problem is to solve for $G_1(r, g_1, g_2,...; \mathrm{Re}_a) = 0$, with $g_2 = g_3 = \cdots = 0$ and with appropriate boundary conditions. The second-order problem is to solve $G_1 = 0$ and $G_2 = 0$ simultaneously with $g_3 = g_4 = \cdots = 0$ and with appropriate boundary conditions. The procedure continues to higher-order problems until the satisfactory convergence criteria between succeeding approximate solutions are obtained.

The (nth)-order problem leads to the system of n fourth-order nonlinear ordinary differential equations in terms of g_1, g_2, etc. as follows:

$$\begin{aligned} &g_n'''' + \frac{2}{r} g_n''' - \frac{2n^2+1}{r^2} g_n'' + \frac{2n^2+1}{r^3} g_n' + \frac{n^4 - 4n^2}{r^4} g_n \\ &+ \frac{\mathrm{Re}_a}{2r} \sum_{m=1}^{N} m \left\{ g_m \left[g_{m+n}''' + \frac{1}{r} g_{m+n}'' - \frac{1+(m+n)^2}{r^2} g_{m+n}' + \frac{2(m+n)^2}{r^3} g_{m+n} \right) \right. \\ &- \left(g_{m-n}''' + \frac{1}{r} g_{m-n}'' + \frac{1+(m-n)^2}{r^2} g_{m-n}' + \frac{2(m-n)^2}{r^3} g_{m-n} \right) \Big] \\ &\left. - \left(g_m'' + \frac{1}{r} g_m' - \frac{m^2}{r^2} g_m \right) (g_{m+n}' - g_{m-n}') \right\} = 0, \end{aligned} \tag{12}$$

with appropriate boundary conditions

$$g_1(r) \sim r \qquad \text{as} \quad r \to \infty, \tag{13}$$

$$g_n(r) = 0, \qquad n = 2, 3,..., N, \tag{14}$$

$$g_n'(r) = 0, \qquad n = 2, 3,..., N, \tag{15}$$

where primes denote differentiation with respect to r, and $g_0 = 0$, $g_{-k} = -g_k$. This system is to be integrated numerically after being reduced to a system of first-order ordinary differential equations.

The first-order problem leads identically to the Stokes approximation and the

associated nonuniformity at infinity, discussed in [30]. This anomaly disappears in the higher order approximations.

Due to limited computer capacity, we consider only six terms in the Fourier series. The accuracy of the surface quantities are to be improved by Shanks' approximation.

4. Third-Order Boundary Conditions at Great Distance

The outer matched asymptotic expansion of the velocity and pressure are assumed to have the form [3, 4]

$$\mathbf{V} = \mathbf{i} + \varepsilon \mathbf{V}_1 + \varepsilon^{3/2}\mathbf{V}_{3/2} + \varepsilon^2 \log \varepsilon \mathbf{V}_{1a} + \varepsilon^2 \mathbf{V}_2 + \cdots . \tag{16}$$

$$p = \varepsilon \tilde{p}_1 + \varepsilon^{3/2}\tilde{p}_{3/2} + \varepsilon^2 \log \varepsilon \tilde{p}_{1a} + \varepsilon^2 \tilde{p}_2 + \cdots , \tag{17}$$

where the V's and $\tilde{p}$'s in the right-hand side of (16) and (17) are respectively, first- to higher order terms and ε is the small parameter

$$\varepsilon = a/R. \tag{18}$$

Here R is an artificial length scale. The velocity and related stream function terms are given in more detail in [10];

$$\begin{aligned} u_\theta(r,\theta) = {} & \left\{1 - \frac{\log \varepsilon}{r^2}\left[\frac{3^{1/2}C_D^3\,\mathrm{Re}_a}{16\pi^2} - \frac{C_D^2}{2\pi^2}\right]\right\}\sin\theta \\ & + \frac{\mathrm{Re}_a^{1/2}\,C_D^2}{8(2\pi r)^{1/2}\,r}\sum_{n=1}^{\infty}\frac{8n(-1)^{n+1}}{\pi(4n^2-1)}\sin n\theta, \end{aligned} \tag{19}$$

$$\begin{aligned} \psi(r,\theta) = {} & \left\{r + \frac{\log \varepsilon}{r}\left[\frac{3^{1/2}C_D^3\,\mathrm{Re}_a}{16\pi^2} - \frac{C_D^2}{2\pi^2}\right]\right\}\sin\theta \\ & - \frac{\mathrm{Re}_a^{1/2}\,C_D^2}{4(2\pi r)^{1/2}}\sum_{n=1}^{\infty}\frac{8n(-1)^{n+1}}{\pi(4n^2-1)}\sin n\theta \\ & - \frac{C_D}{2\pi}\sum_{n=1}^{\infty}\frac{2}{n}(-1)^{n+1}\sin n\theta, \end{aligned} \tag{20}$$

where C_D is total drag coefficient. From (19) and (20), we find the following conditions at infinity for the expansions of $\psi(r,\theta)$ and $u_\theta(r,\theta)$

$$g_1(r) = r + \frac{\log \varepsilon}{r}\left[\frac{3^{1/2}C_D^3\,\mathrm{Re}_a}{16\pi^2} - \frac{C_D^2}{2\pi^2}\right] - \left(\frac{\mathrm{Re}_a}{2\pi}\right)^{1/2}\frac{C_D^2}{r^{1/2}}\frac{2}{3\pi} - \frac{C_D}{\pi}, \tag{21}$$

$$g_1'(r) = 1 - \frac{\log \varepsilon}{r^2}\left[\frac{3^{1/2}C_D^3\,\mathrm{Re}_a}{16\pi^2} - \frac{C_D^2}{2\pi^2}\right] + \left(\frac{\mathrm{Re}_a}{2\pi}\right)^{1/2}\frac{C_D^2}{r^{3/2}}\frac{1}{3\pi}, \tag{22}$$

$$g_n(r) = (-1)^n \left[\left(\frac{\mathrm{Re}_a}{2\pi r} \right)^{1/2} \frac{2nC_D^2}{(4n^2-1)\,\pi} + \frac{C_D}{n\pi} \right], \qquad n = 2, 3,..., \tag{23}$$

$$g_n'(r) = (-1)^{n+1} \left[\left(\frac{\mathrm{Re}_a}{2\pi r} \right)^{1/2} \frac{nC_D^2}{(4n^2-1)\,\pi r} \right], \qquad n = 2, 3,.... \tag{24}$$

In the actual numerical solution, (21)–(24) are used as the boundary conditions imposed at a sufficiently large distance from the surface of the cylinder instead of using (15) as mentioned toward the end of Section 2.

5. Drag and Pressure Coefficients and Separation Angle

The drag coefficient based on frontal area has been the most closely examined flow property. The present semianalytic method gives a simple expression for the calculation of friction, pressure, and total drag coefficients,

$$C_{D_F} = (2\pi/\mathrm{Re}_a)\, g_1''(1), \tag{25}$$

$$C_{D_P} = -(2\pi/\mathrm{Re}_a)[g_1'''(1) + g_1''(1)], \tag{26}$$

$$C_D = -(2\pi/\mathrm{Re}_a)\, g_1'''(1). \tag{27}$$

It is seen that only the first term in the Fourier expansion of $\psi(r, \theta)$ contributes to the drag coefficient. Naturally, because of the ellipticity of the equations, the values of $g_1(1)$ and its derivatives do change as the number of terms in Eq. (9) is increased.

The pressure coefficient may be calculated by integration of the governing equations, and is given by

$$\begin{aligned} C_P &\equiv (\text{Dimensional}(P_\theta - P_\infty)/\tfrac{1}{2}\rho U_\infty^2 \\ &= \frac{2}{\mathrm{Re}_a} \left\{ \sum_{n=1}^{\infty} \frac{1}{n} [g_n'''(1) + g_n''(1)][1 - \cos n\theta] \right\} \\ &\quad + \frac{2}{\mathrm{Re}_a} \int_{r=1}^{\infty} \left\{ \sum_{n=1}^{N} \frac{n}{r} \left[g_n''(r) + \frac{1}{r}\, g_n'(r) - \frac{n^2}{r^2}\, g_n(r) \right] \right\} dr \\ &\quad + 2 \int_{r=1}^{\infty} \left\{ \sum_{n=1}^{N} \frac{n}{r}\, g_n(r) \right\} \left\{ \sum_{n=1}^{N} \left[\frac{n}{r}\, g_n'(r) - \frac{n}{r^2}\, g_n(r) \right] \right\} dr. \end{aligned} \tag{28}$$

The position at which the vorticity changes sign indicates the flow separation point. The flow separation angle (measured from the rear stagnation point) is seen in the computation to increase with increasing Reynolds number.

At the point of separation, vorticity vanishes and the angle of separation $\theta = \pi - \theta_s$ may be found from the root of (5) when we set $r = 1$ and $\omega = 0$:

$$\sum_{n=1}^{\infty} g_n''(1) \sin n\theta = 0, \tag{29}$$

where θ_s is the separation angle measured from the rear stagnation point.

6. Initial Value Adjusting Method with Interval Decomposition

Several numerical techniques have been investigated for the solution of the present two-point boundary value problem of nonlinear ordinary differential equations. The quasilinearization technique introduced by Bellman and Kalaba [2] has some disadvantages. First, the partial derivatives of the system equation (the Jacobian mtrix) must be evaluated analytically. Second, selection of the first approximation which leads to convergence is, in general, difficult. Third, storage of the previous iteration procedure is required. The modified quasilinearization technique developed by Baird [1] reduces the computer storage, but it is necessay to solve an additional linear boundary value problem. The technique of Lentini and Pereyra [13] has again the same disadvantage as Bellman and Kalaba's method.

The initial value adjusting method with interval decomposition for the solution of nonlinear multipoint boundary value problems (MPBVP) of nonlinear ordinary differential equations by Ojika [16], being simple and efficient, has been adopted for the present two-point boundary value problem.

In this technique, the original MPBVP was transformed into a set of initial value subproblems. From the solution of each initial value subproblem with a set of slightly perturbed initial conditions (from the previous initial conditions), one calculates corresponding variations of the nonlinear conditions. Then by the initial value adjusting method [17, 18], a set of new initial conditions was determined in order to satisfy simultaneously the given boundary conditions and continuity conditions at the boundary points. The quadratic convergence property of this method has the advantage of small computer storage requirements. This method deals directly with the original differential equations and the given boundary conditions, so it is not necessary to use the solutions of additional linear equations or to evaluate analytically the partial derivatives of the given equations.

Consider the system of n-dimensional nonlinear ordinary differential equations as the nonlinear multipoint, or in the special case, two-point, boundary value problems,

$$dx(t)/dt = f(x, t), \qquad t_1 \leqslant t \leqslant t_m, \tag{30}$$

subject to nonlinear or linear boundary conditions

$$g[x(t_1), x(t_2), \ldots, x(t_m)] = 0, \qquad t_1 < t_2 < \cdots < t_m, \quad m \geqslant 2, \tag{31}$$

where t is the independent variable and t_ρ ($\rho = 1, 2,..., m$) is fixed, $x(t)$ is an n-vector, f is an n-vector function twice continuously differentiable with respect to x and continuous in t within the interval $[t_1, t_m]$, and g is an n-vector function twice differentiable with respect to each $x(t_\rho)$ ($\rho = 1, 2,..., m$).

Instead of solving (30) and (31), we decompose the overall interval $[t_1, t_m]$ into $m-1$ subintervals and solve a set of initial value problems

$$\frac{d^{k+1}x^{(\rho)}(t)}{dt} = f({}^{k+1}x^{(\rho)}, t), \tag{32}$$

$${}^{k+1}x^{(\rho)}(t_\rho^+) = {}^{k+1}x^{(\rho)}, \qquad t_\rho < t < t_{\rho+1}, \quad \rho = 1, 2,..., m-1 \tag{33}$$

with corresponding boundary conditions

$${}^{k+1}g = g[{}^{k+1}x^{(1)}(t_1^+),..., {}^{k+1}x^{(m-1)}(t_{m-1}^+), {}^{k+1}x^{(m-1)}(t_{m-1}^-)] = 0, \tag{34}$$

where the superscript $k+1$ refers to the $(k+1)$th step of the iteration and (ρ) refers to the ρth subinterval. The plus and minus signs in (34) refer to the right and left limits of t, respectively. In addition, the continuity condition must be satisfied at each boundary point

$${}^{k+1}x^{(\rho)}(t_\rho^+) - {}^{k+1}x^{(\rho-1)}(t_\rho^-) = 0, \qquad \rho = 2, 3,..., m-1. \tag{35}$$

Equation (32) for the ρth subinterval at the kth step of the iteration may be written as

$$d\,{}_j^k y^{(\rho)}(t)/dt = f({}_j^k y^{(\rho)}, t), \qquad {}_j^k y^{(\rho)}(t_\rho^+) = {}^k x^{(\rho)}(t_\rho^+) + \varepsilon e_j, \tag{36}$$

$$t_\rho < t < t_{\rho+1}, \qquad j = 1, 2,..., n, \quad \rho = 1, 2,..., m-1, \tag{37}$$

where ${}_j^k y^{(\rho)}$ denotes an n-dimensional vector, ε is a small perturbation parameter, and e_j denotes the jth unit vector given by $e_j = (0,..., 1,..., 0)$. The solution of (36) sets the new initial conditions at each subinterval. The procedure will be terminated if the convergence condition at the kth iteration defined by

$$k_G = [{}^k\beta\,{}^k\beta/n(m-1)]^{1/2} < \varepsilon' \tag{38}$$

is satisfied, where the convergence criterion ε' is given by the user and ${}^k\beta$ is defined by

$${}^k\beta = \begin{bmatrix} {}^k g \\ {}^k x^{(2)}(t_2^+) - {}^k x^{(1)}(t_2^-) \\ \vdots \\ {}^k x^{(m-1)}(t_{m-1}^+) - {}^k x^{(m-2)}(t_{m-1}^-) \end{bmatrix}, \qquad k = 0, 1,.... \tag{39}$$

There are some observations about the method and the algorithm:

(1) The algorithm given is valid for decomposition at arbitrary points.

(2) The number of subintervals remains constant throughout the entire computations if the convergence criteria can be satisfied. Otherwise all the subintervals are further decomposed automatically into two equal subintervals.

(3) The initial value subproblems are solved by the Runge–Kutta–Gill method [7].

In all truncations, we let $\varepsilon' = 10^{-5}$; convergence criteria for the subroutines MPIVID (multipoint boundary value problems–initial value adjusting method with interval decomposition) and GAUSSD (Gauss elimination) are 10^{-5} and 10^{-12}, respectively.

The boundary conditions at infinity were imposed as a sufficiently large distance from the surface of the cylinder. This distance changes with the Reynolds number of the flow.

The numerical computations in the present investigation were programmed in FORTRAN IV (G-level) for solution in the IBM 370/158 automatic digital computer and DEC-10 at the University of Southern California. Typical machine times were 2, 4, 8, 13, and 19 minutes for second through sixth truncations, respectively.

7. Discussion of Results

Results of the Present Study

Results have been obtained for Reynolds numbers ranging from 0.4 to 40. An outer boundary of 91 times and 41 times the radius of the cylinder for Reynolds numbers between 0.4 and 10 and between 15 and 40, respectively, were chosen. As a test of the outer boundary, radii r_∞ of 41, 61, and 91 times the radius of the cylinder for $\mathrm{Re} = 10$ were selected. It is seen from the results that little change has occurred. For consistent results, the outer boundary at infinity was set the same in all truncations for a given Re.

In the application of the method of series truncation, the numerical convergence of successive truncations is of primary importance. The term *convergence* in the present text refers to the quadratic convergence for the initial value adjusting method discussed in Section 6.

As will be seen later in Fig. 6, in which the drag coefficient is plotted versus Reynolds numbers ranging from 0.4 to 40 for the second to sixth truncations, additional terms in the Fourier series would yield a more accurate drag coefficient. Because of the limited capacity of the computer, adding more terms in the Fourier series was not feasible. Applying the nonlinear Shanks' transformation [22], however, the accurate calculation of the drag coefficient for each Reynolds number becomes

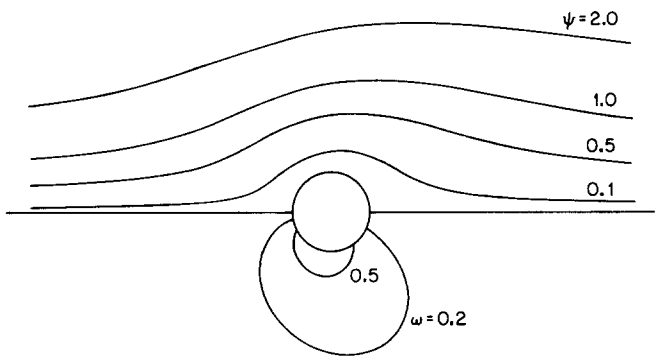

FIG. 1. Streamlines and equi-vorticity lines from the sixth truncation at Re = 1.

possible. If S_{n-1}, S_n, and S_{n+1} represent three successive approximations to a quantity, a revised value is given by

$$e_1(S_n) = (S_{n+1}S_{n-1} - S_n^2)/(S_{n+1} + S_{n-1} - 2S_n). \tag{40}$$

The application of this transformation to each of the three successive truncations yields the final value to three significant figures. This transformation is also applied to the other surface quantities, but not the field quantities.

Since the sixth truncation yields the best obtainable approximation without the application of Shanks' transformation, the stream function (9), vorticity (5), and velocity profiles have been plotted based on it. The corresponding streamlines and equi-vorticity lines are plotted on the top and bottom of the cylinder. Figure 1 shows the flow pattern for Reynolds number 1. In the course of computation the bubble

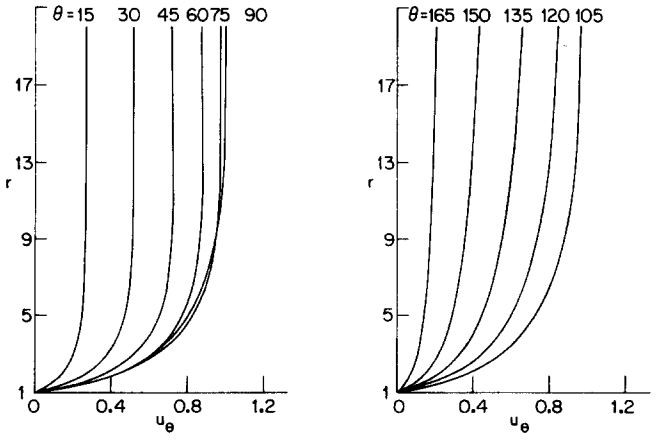

FIG. 2. Tangential velocity from the sixth truncation at Re = 1.

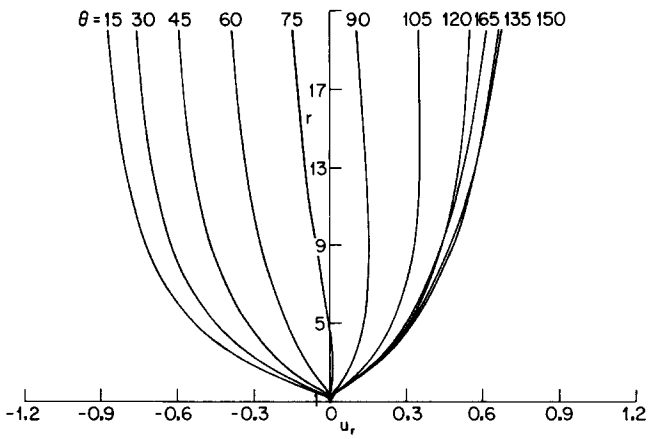

FIG. 3. Radial velocity from the sixth truncation at Re = 1.

begins to appear at Re = 7. As the Reynolds number increases, the bubble or recirculating region behind the cylinder grows. At low Reynolds numbers the streamlines display fore-and-aft symmetry close to the surface, as in Fig. 1.

The components of tangential velocity (4) versus angle are plotted in Fig. 2 for Re = 1. The figure shows the velocity profiles along the surface and displays fore-and-aft symmetry with respect to the top of the cylinder for low Reynolds number. In the thin viscous layer, the velocity increases from zero to a maximum then decreases to the free stream value.

The components of radial velocity (3) versus angle for the same Reynolds numbers are shown in Fig. 3. The radial velocity components begin at zero on the cylinder surface and approach that of the free stream

$$u_r \to -\cos\theta \qquad \text{as} \quad r \to \infty. \tag{41}$$

In Figs. 4 and 5, Shanks' extension of the pressure coefficient and surface vorticity

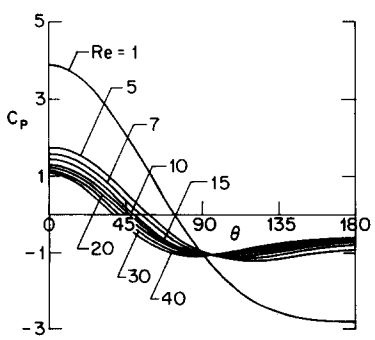

FIG. 4. Pressure coefficient calculated from the Shanks' extension at various Reynolds numbers.

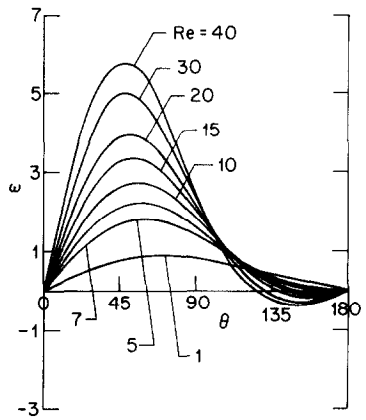

FIG. 5. Vorticity distribution on the cylinder calculated from the Shanks' extension at various Reynolds numbers.

are plotted versus the angle, as the Reynolds numbers change.

In Fig. 6 we show the drag coefficient from the second to sixth truncations as well as Shanks' extension for each quantity.

Comparison of Results

In Figs. 7 and 8, the predicted surface vorticities from the present study are compared with other authors' numerical solutions at Reynolds numbers 1 and 40, respectively. The values plotted in Fig. 7 show very good agreement with Nieuwstadt and Keller at $\mathrm{Re} = 1$. In Fig. 8 the results are in good agreement with those of

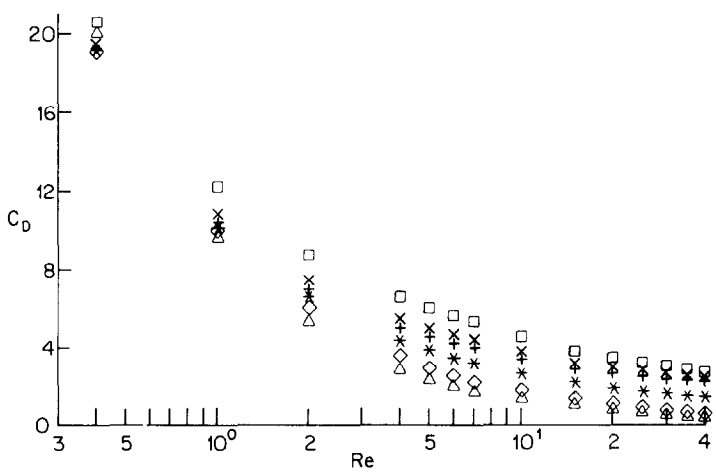

FIG. 6. Total drag coefficient versus Reynolds number from the different truncations and Shanks' extension: second (□), third (△), fourth (×), fifth (◇), and sixth truncations (+); (∗) Shanks' extension.

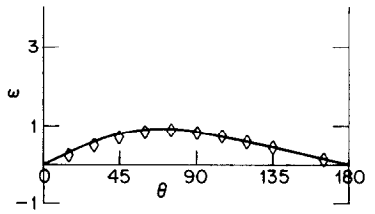

FIG. 7. Vorticity distribution on the cylinder from the sixth truncation, Shanks' extension, and other numerical solutions at Re = 1: (◇), Nieuwstadt and Keller [15]; (---), sixth truncation; and (—), Shanks' extension.

Dennis and Chang [5], Nieuwstadt and Keller, and recent computation by Fornberg [6] at Reynolds number 40.

In Table I the drag coefficient is also compared with existing numerical solutions. In Table II the separaion angle is presented and the result is in good agreement with numerical solutions of Dennis and Chang, Nieuwstadt and Keller, Takami and Keller, and the finite element method of Tuann and Olson for Reynolds numbers between 10 and 40. Hamielec and Raal [9], Fornberg, and Underwood show higher values. In Fig. 9, the total drag coefficient of the present study has been compared with existing experimental data. The result is in good greement with those of Wieselberger [31], Relf [21], and Tritton [26] for high Reynolds numbers and differs slightly from those of Tritton at low Reynolds numbers.

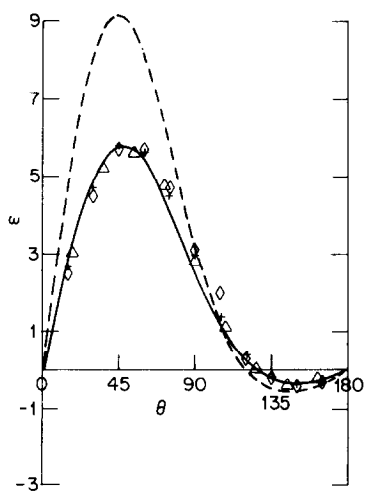

FIG. 8. Vorticity distribution on the cylinder from the sixth truncation, Shanks' extension, and other numerical solutions at Re = 40: (+), Dennis and Chang [5]; (◇), Nieuwstadt and Keller [15]; (△), Fornberg [6]; (---), sixth truncation; and (—), Shanks' extension.

TABLE I

Comparison of Total Drag Coefficient from the Sixth Truncation and Shanks' Extension with Existing Numerical Solutions

Re	Takami and Keller (1969)	Underwood (1969)	Hamielec and Raal (1969)	Dennis and Chang (1970)	Nieuwstadt and Keller (1973)	Tuann and Olson (1978)[a]	Fornberg (1980)	Sixth truncation (present)	Shanks' extension (present)
0.4	—	19.225	—	—	—	—	—	19.284	19.233
1	10.283	—	10.97	—	10.3129	14.013	—	10.438	10.276
2	6.637	—	6.83	—	—	—	—	6.991	6.358
4	4.439	—	4.52	—	—	—	—	4.993	4.342
5	—	—	—	4.116	—	4.661	—	4.439	3.828
6	3.565	—	—	—	—	—	—	4.217	3.462
7	3.303	—	—	3.421	3.4133	3.849	—	3.976	3.186
10	2.80	3.5	2.75	2.846	2.8283	3.177	—	3.506	2.647
15	2.265	—	2.27	—	—	—	—	2.866	2.211
20	2.013	—	—	2.045	2.053	2.253	2.0001	2.644	1.927
30	1.717	—	1.588	—	1.7329	—	—	2.382	1.600
40	1.536	—	—	1.522	1.5504	1.675	1.498	2.224	1.555

[a] Finite element method, 78 elements.

TABLE II

Comparison of Separation Angle from the Sixth Truncation and Shanks' Extension with Existing Numerical Solutions

Re	Takami and Keller (1969)	Underwood (1969)	Hamielec and Raal (1969)	Dennis and Chang (1970)	Nieuwstadt and Keller (1973)	Tuann and Olson (1978)[a]	Fornberg (1980)	Sixth truncation (present)	Shanks' extension (present)
5	—	—	—	—	—	>6°	—	—	—
7	14.5°	—	—	15.9°	—	22.7°	—	22.67°	11.788°
10	29.3°	30.0°	32.4°	29.6°	27.96°	29.7°	30.55°	34.86°	20.278°
15	38.7°	—	40.6°	—	—	—	—	43.09°	36.103°
20	43.65°	—	—	43.7°	43.37°	44.1°	45.14°	48.60°	41.333°
30	49.6°	—	52.7°	—	49.38°	—	—	55.80°	47.032°
40	53.55°	—	—	53.8°	53.34°	54.8°	55.21°	60.96°	51.422°

[a] Finite element method, 78 elements.

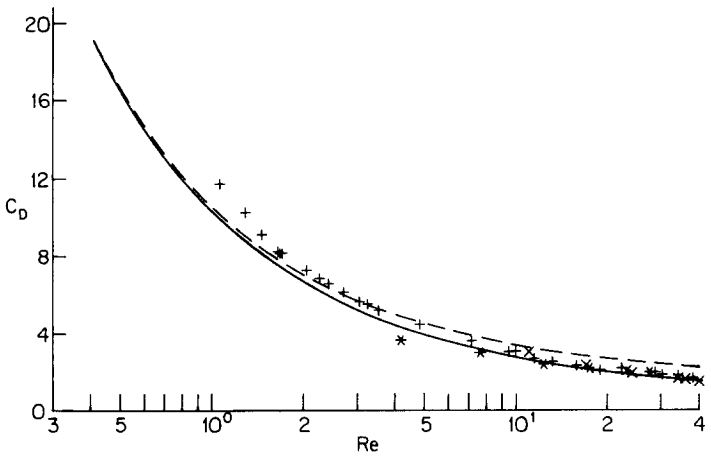

FIG. 9. Comparison of total drag coefficient versus Reynolds number from the sixth truncation and Shanks' extension with existing experimental data: (×), Relf [21]; (*), Wieselberger [31]; (+), Tritton; (---), sixth truncation; and (—), Shanks' extension.

8. CONCLUSIONS AND DISCUSSION

The main objective of the present work has been to investigate the steady viscous incompressible flow past a circular cylinder. The series truncation method has been applied to the full Navier–Stokes equations. Fourier series expansion (9) has been chosen for the stream function and is valid throughout the domain of interest. The asymptotic behavior of the flow at infinity has been carefully studied.

Numerical solutions for the steady viscous incompressible flow past a circular cylinder have been presented by the series truncation method for a range of Reynolds numbers from 0.4 to 40. Because the sixth truncation solutions yield a better approximation than the lower truncations (as expected), the flow pattern and tangential and radial velocities have been plotted for the sixth truncation. The surface characteristics of flow, such as the pressure coefficient, surface vorticity, drag coefficient, and separation angle using Shanks' transformation are found to be in consistent agreement with those of Nieuwstadt and Keller [15], Dennis and Chang [5], and a recent computation by Fornberg [6] for the present Reynolds number range. The drag coefficient was also found in good agreement with Tritton's [26] data. The present computation shows that the closed wake length (s) appears at Reynolds numbers between 5 and 7.

APPENDIX: NOMENCLATURE

a	Radius of the cylinder
C_D	Total drag coefficient
C_{D_F}	Friction drag coefficient
C_{D_P}	Pressure drag coefficient
d	Diameter of the cylinder
P	Pressure
P_∞	Pressure at infinity
r	Radial coordinate
Re	Reynolds number
S	Wake length
U_∞	Free stream velocity
$u_r(r, \theta)$	Radial velocity $= -(1/r)\,\partial\psi(r, \theta)/\partial\theta$
$u_\theta(r, \theta)$	Tangential velocity $= \partial\psi(r, \theta)/\partial r$
ε'	Convergence criterion
θ	Angular coordinate
θ_s	Separation angle
μ	Viscosity = const
ν	Kinemtic viscosity $= \mu/\rho$
ρ	Density
ψ	Stream function
ω	Vorticity

REFERENCES

1. C. A. BAIRD, *J. Optim. Theory Appl.* **3** (1969), 227.
2. R. E. BELLMAN AND R. E. KALABA, "Quasilinearization and Nonlinear Boundary-Value Problems," Amer. Elsevier, New York, 1965.
3. I. D. CHANG, *J. Math. Phys.* **10** (1961), 811.
4. I. D. CHANG, private communication, 1980.
5. S. C. R. DENNIS AND GAU-ZU CHANG, *J. Fluid Mech.* **42** (1970), 471.
6. B. FORNBERG, *J. Fluid Mech.* **98** (1980), 819.
7. S. GILL, *Proc. Cambridge Philos. Soc.* **47** (1951), 96.
8. I. IMAI, *Proc. R. Soc. London, Ser. A* **208** (1951), 437.
9. A. E. HAMIELEC AND J. D. RAAL, *Phys. Fluids* **12** (1969), I-11.
10. H. JAFROUDI, "Computation of Steady Laminar Flow over a Circular Cylinder with Third-Order Boundary Conditions," Ph.D. Dissertation, University of Southern California, Los Angeles, 1981.
11. S. KAPLUN, *J. Math. Mech.* **6** (1957), 595.
12. M. KAWAGUTI, *J. Phys. Soc. Japan* **8** (1953), 747.
13. M. LENTINI AND V. PEREYRA, *SIAM J. Numer. Anal.* **14** (1977), 91.
14. L. M. MILNE-THOMSON, "Theoretical Hydrodynamics," 5th ed. p. 646, Macmillan, New York, 1968.
15. F. NIEUWSTADT AND H. B. KELLER, *Comput. Fluids* **1** (1973), 59.

16. T. OJIKA, "Multipoint Boundary-Value Problems for Non-Linear Ordinary Differential Equations (Initial-Value Adjusting Methods with Interval-Decomposition)," The Scientific Subroutine Library, Kyoto University, Kyoto, Japan, 1978.
17. T. OJIKA, *J. Math. Anal. Appl.* **73** (1980), 192.
18. T. OJIKA AND Y. KASUE, *J. Math. Anal. Appl.* **69** (1979), II-359.
19. C. W. OSEEN, *Ark. Mat. Astron. Fys.* **6** (1910), 1.
20. I. PROUDMAN AND J. R. PEARSON, *J. Fluid Mech.* **2** (1957), 237.
21. E. F. RELF, *Brit. A. R. C. Rep. Memo.*, No. 102, (1914).
22. D. SHANKS, *J. Math. Phys.* **34** (1955), 1.
23. G. G. STOKES, *Trans. Cambridge Philos. Soc.* **9** (1851), 8; reprinted in *Math. Phys. Papers* **3** (1901), 1, Cambridge Univ. Press, London/New York.
24. H. TAKAMI AND H. B. KELLER, *Phys. Fluids Suppl. II*, **12** (1969), II-5.
25. A. THOM, *Proc. R. Soc.* **141** (1933), 651.
26. D. TRITTON, *J. Fluid Mech.* **6** (1959), 547.
27. S. Y. TUANN AND M. D. OLSON, *Comput. Fluids* **5** (1978), 219.
28. R. L. UNDERWOOD, *J. Fluid Mech.* **36** (1969), 95.
29. M. D. VAN DYKE, *in* "Proceedings, 11th International Congress of Applied Mechanics," p. 1165, 1966.
30. M. D. VAN DYKE, "Perturbation Method in Fluid Machanics," Stanford, the ParabolicPress, Stanford, Calif., 1975.
31. C. WIESELBERGER, *Phys. Z.* **22** (1929), 32; **23** (1921), 219.